JOURNAL OF MECHANICAL ENGINEERING AND SCIENCES (JMES)
ISSN: 2289-4659 e-ISSN: 2231-8380
VOL. 16, ISSUE 3, 9033 – 9042
DOI: https://doi.org/10.15282/jmes.16.3.2022.06.0715

ORIGINAL ARTICLE

Effect of gable roof with various roof pitches and obstacle heights on natural ventilation performance for an isolated building

A.A. Zobaied[1], V.C. Tai[2,], T.F. Go[3], P.L. Chong[4], and L.K. Moey[2]

[1] Faculty of Engineering, Built Environment & Information Technology, SEGi University, 47810, Selangor, Malaysia.
[2] Centre for Modelling and Simulation, Faculty of Engineering, Built Environment & Information Technology, SEGi University, 47810, Selangor, Malaysia.
Phone: 03-6145 1777; Fax.: 03-6145 1666
[3] Centre for Advance Materials and Intelligent Manufacturing, Faculty of Engineering, Built Environment & Information Technology, SEGi University, 47810, Selangor, Malaysia.
[4] School of Computing, Engineering & Digital Technologies, Teesside University, Middlesbrough, TS1 3BX, United Kingdom.

ABSTRACT – Numerical analysis based on CFD steady RANS equations was used to study the airflow characteristics around and within an isolated gable roof building. Parameters that are the main study focus of this research include: streamlines of normalized velocity, pressure coefficient and ventilation rate. The effect of gable roof with four different roof pitches namely 15º, 25º, 35º & 45° were investigated against varying obstacle heights of 40, 50, 60 & 70 mm. From the simulation results, the streamlines show that larger roof pitch leads to increased velocity at the window and roof openings due to the external and internal pressure difference in the building. The corresponding increment in internal obstacle height on the other hand leads to gradual alteration of airflow direction in front of the obstacle, and also an increase of the pressure coefficient inside the building because of wind blocking effect. This pressure coefficient also sees a reduction in value at the windward and inside of the building with an increase in steepness of the roof pitch due to increasing internal velocity. Hence, airflow behavior and characteristics are clearly dependent on roof pitch and internal obstacle height which indicates a good agreement with the findings from the previous studies. Gable roof with a steeper roof pitch building coupled with lower internal obstacle height will therefore yield better ventilation rates.

ARTICLE HISTORY
Received: 15th Jan. 2022
Revised: 10th Apr. 2022
Accepted: 13th May 2022

KEYWORDS
Gable roof
Roof pitch
Obstacle height
CFD
Ventilation rate

INTRODUCTION

Natural ventilation is an emerging key in reducing energy demands in built environments that can achieve promising energy efficiency and sustainability requirements. Energy efficiency of a building can be improved by optimizing the building form, ceiling, building orientation and façade design [1]. Natural ventilation uses wind force and air density differential to drive fresh air into a building, and subsequently repels aged air to the outside without the assistance of mechanical systems. It provides a highly effective and ecological passive cooling mechanism by introducing clean fresh air into a space [2, 3]. A properly designed roof configuration is one of the major factors that contribute to the energy efficiency in buildings as it accounts for up to 50% of a building's solar energy gain [4]. Roof configuration also has significant impact on the wind flow pattern around and within a building [5–7]. Typical roof types include hip, venturi, and gable configurations.

A measure of building ventilation performance can be conducted by using several methods such as experiments, analytical, semi empirical formula, and simulations [5,7]. In the past decade, numerical analysis based on computational fluid dynamics (CFD) has become the mainstream method in evaluating building ventilation performance [5, 8]. As compared to conventional methods, CFD provides complete flow field data, allows customizations of model scales and also full control over the boundary conditions; therefore, allowing the study of building ventilation performance to be carried out more efficiently. For these reasons, CFD was employed in most studies on the evaluation and enhancement of building ventilation performance [5].

Gable roof is one of the most classic and frequently used roof shapes around the world [9]. It is used both in snowy regions for snow drifting prediction purposes, as well as in hot and humid climate for its proven positive effects on natural ventilation [10]. Tominaga et al. [8] performed wind tunnel experiments and CFD simulations to understand the airflow characteristics around an isolated gable roof building. This study confirmed that gable roof pitch affects the streamlines, distribution of turbulent kinetic energy (TKE), pressure coefficient, and U/U_{ref} around the building. Moey et al. conducted a numerical study to investigate the ventilation performance of an isolated building with a gable roof and various roof pitches namely 15°, 25° & 35°. The numerical results showed the ventilation rate inside the building increases with the increment in roof pitches [11]. Zhou et al. [9] analysed the impact of gable roof inclination on snow distribution with a series of two-dimensional CFD simulations and wind tunnel experiments. According to his study, gable roof can be categorized into two categories namely that of low slope (0˚ to 15˚ roof pitch) and high slope (15˚ roof pitch and above).

*CORRESPONDING AUTHOR | L.K. Moey | ✉ moeylipkean@segi.edu.my

This roof slope affects the separation of flow at the leading edge and roof ridge, which subsequently affects the ventilation performance. Chu & Chiang [12] also jointly conducted a study to evaluate the wind-driven cross ventilation through low rise building with internal obstacles using the LES model and wind tunnel experiment. Both experimental and numerical findings consistently showed that the ventilation rate reduces when an obstacle is placed adjacent to any inlet or outlet opening. In other words, the resistance of flow will increase as distance between the aforementioned obstacle and the opening decreases. To the best of authors' knowledge, the study focuses on the impact of roof configuration with internal obstacle on indoor natural ventilation has yet to be carried out in the literature. Hence, the focus of this research is to study the effect of gable roof pitches in an isolated naturally ventilated building having different obstacle heights. The generated results of the numerical simulation are then compared with the experimental and numerical studies carried out by Karava et al. [13] and Ramponi and Blocken [5], respectively.

This paper is further divided into several different sections. Section 2 describes the description of the experiment. Section 3 defines numerical setting and parameters, grid sensitivity study as well as model validation based on the wind tunnel experiments by Karava et al. [13] and numerical study by Ramponi and Blocken [5]. Moreover, gable roof model validation is based on the simulation results by Tominaga et al. [8]. Section 4 addresses the results of simulation for the gable roof building with different roof pitches and obstacle heights, and also the discussion on the effect of various gable roof pitches with different obstacle heights on airflow characteristics. Lastly, the findings of this study will be concluded in section 5.

DESCRIPTION OF THE EXPERIMENT

Karava et al. [13] conducted the comprehensive Particle Image Velocimetry (PIV) measurements to evaluate the natural ventilation for an isolated building with a boundary layer wind tunnel. The open-circuit wind tunnel has a length of 12 m and a cross sectional area of 1.8 × 1.8 m^2, while the building model has dimensions of 0.1 m × 0.1 m × 0.08 m (length × width × height) that corresponds with full scale dimensions of 20 m × 20 m × 16 m. This reduced scale model undergo the CFD simulation conducted by Ramponi and Blocken [5]. The result obtained was compared and accuracy were verified. Figure 1 illustrates the dimensions of the building model. In this paper, the model with both windward and leeward openings located at the center and with a wall porosity (ratio between the opening area and the area of the wall) of 10% was referred [5, 13].

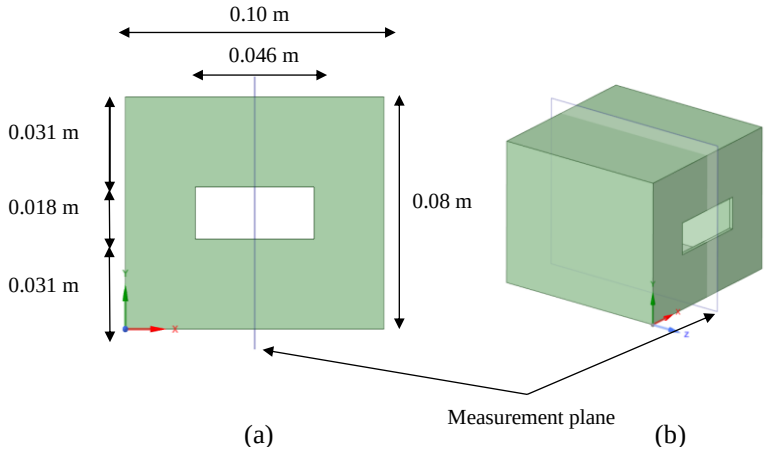

Figure 1. (a) Dimensions for the front view of the model and (b) measurement plane of reference building model [13]

The building model was positioned in the glass window extension and orientated with openings perpendicular to the incoming flow. The floor was covered using extruded polystyrene (XPS) and carpeted along the wind tunnel to reproduce an open terrain roughness profile. The aerodynamic roughness length of z_0 = 0.025 mm in reduced scale, equating to 0.005 m in real scale [5]. At the reference height, a mean wind speed of 6.97 m/s and turbulence intensity of 10% were measured. These measurements were done in an empty wind tunnel using a hot-film probe. The turbulence intensity near ground level and gradient heights are around 17% and 5%, respectively. The reading of PIV experiments were taken in a horizontal plane through the center of the openings and at a vertical plane of symmetry [13]. The results were used for model validation purpose in this paper.

NUMERICAL STUDY: MODEL SETUP AND CFD SIMULATION

Simulation Case, Computational Domain and Grids

In this research, a reference model for an isolated building was selected. This model has a 1:200 reduced scale dimensions of length × width × height (L × W × H) = 0.1 m × 0.1 m × 0.08 m, that corresponds to the actual dimensions of 20 m × 20 m × 16 m. This model was also configured with a pair of window (h = 18 mm) and roof openings (h = 9 mm) at windward and leeward walls, with y = 0.04 m at the center of the window opening, and y = 0.0655 m above

ground level for the roof opening. The thickness of the wall for the tested model was 2 mm as per Ramponi and Blocken's recommendation [5]. A gable roof with various roof pitches, openings as well as different internal obstacle heights with 2 mm thickness and a fixed length L = 80 mm located at the centerline of the building were added to the building model. The building was tested with four different roof pitches, namely that of 15°, 25°, 35° & 45° plus obstacle heights of 40, 50, 60 & 70 mm. Figure 2 shows the dimensions of the gable roof of 15° roof pitch with obstacle height (h). Table 1 shows the simulation cases with different roof pitches and internal obstacle with different heights conducted in this study.

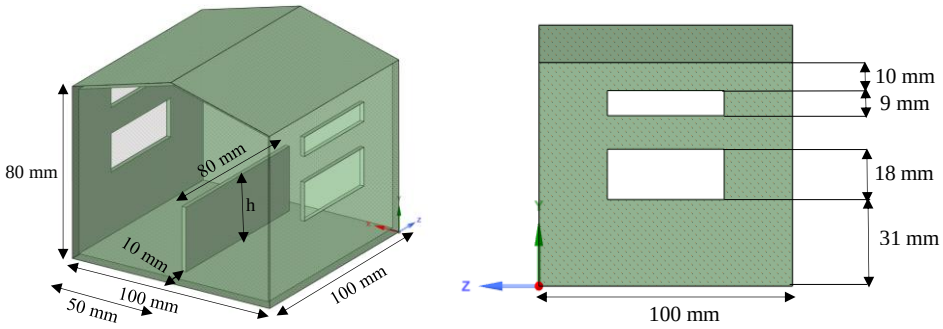

(a) (b)

Figure 2. (a) Dimensions of the gable roof with 15° roof pitch with inernal obstacle and (b) front view of model dimensions

Table 1. Simulation cases of gable roof

Cases	Roof Pitches (°)	Obstacle height, h (mm)
Case 1	15	40
Case 2	25	40
Case 3	35	40
Case 4	45	40
Case 5	15	50
Case 6	25	50
Case 7	35	50
Case 8	45	50
Case 9	15	60
Case 10	25	60
Case 11	35	60
Case 12	45	60
Case 13	15	70
Case 14	25	70
Case 15	35	70
Case 16	45	70

Simulations were performed based on a reduced scale model in representation of the actual building model. The computational domain was generated with reference to the operational guide introduced by Franke et al. [14] and Tominaga et al. [15] with an exception of the distance from the inlet plane of the flow domain to the windward side of the tested model which has been decreased from 5H to 3H to restrict the amount of unintentional streamwise gradient [5]. Figure 3 shows the top and side walls of the computational domain were located 5H apart from the model, whist the downstream length was specified as 15H, of which H is the height of the building at 0.08 m.

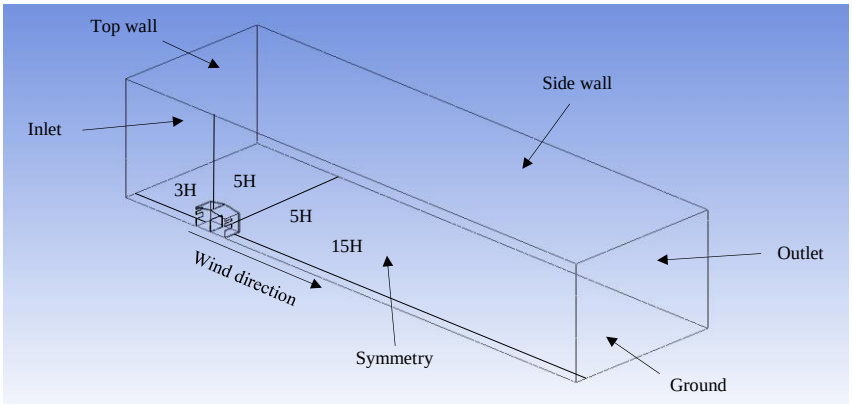

Figure 3. Dimensions of the computational domain

Mosaic™ meshing technology was selected to generate the computational grids. It offers the benefits of producing good quality octree hexahedron in the bulk region, allowing automatic connection of elements despite its type, and delivering high efficiency in solving fluid flow of complex geometries [16]. The Mosaic™ meshing technology also speeds up the solver by 10 – 50% while offering similar results and consuming lesser machine memory. The model geometry and computational domain were first remeshed with tetrahedral elements using the local scope sizing function based on the curvature, proximity, and soft size requirements. The mesh type was then converted into Poly-hexcore type by preserving its average edge length consistency with triangular surface mesh as shown in Figure 4 [16].

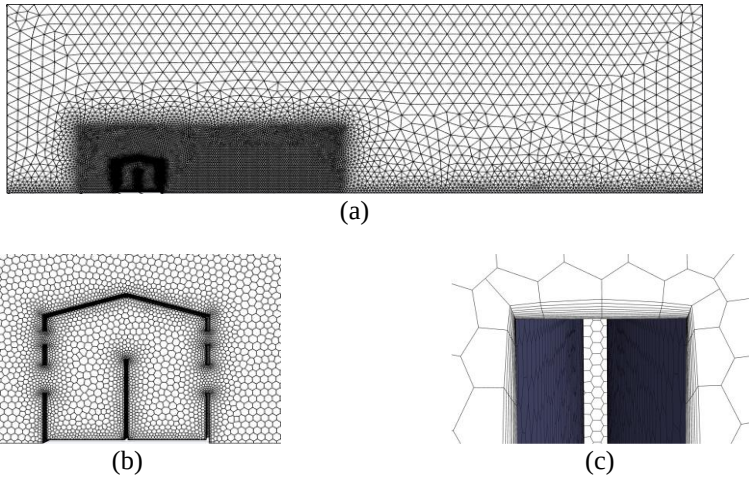

(a) (b) (c)

Figure 4. (a) Triangular surface mesh, (b) Poly-hexcore mesh and (c) inflation layers generated for gable roof building with 15° roof pitch

Boundary Conditions

The boundary condition of measured mean wind speed together with turbulence intensity from the wind tunnel experiment were employed at the inlet plane. The wind velocity profile at the inlet was determined in accordance to the logarithm law with z_0 = 0.025 mm using Eq. (1). whereby the u^*_{ABL} was computed using the reference wind speed, U_{Ref} of 6.97 m/s, reference height, Z_{Ref} of 0.08 m, Von Karman constant, κ of 0.4, and the aerodynamic roughness height Z_0 of 0.00003 m [17]. The mean wind speed U(z) and turbulence intensity I_u (z) were then applied to calculate the turbulent kinetic energy k(z) at reference height by using Eq. (2). Previous studies have been conducted to identify the best value of α [15,18]. As recommended by Tominaga et al. [8], α = 1 was used in this present study. The rate of turbulence dissipation ε and specific dissipation rate ω were calculated by using Eq. (3) and (4), respectively of which C_μ is the empirical constant equivalent to 0.09 which was suggested by Ramponi and Blocken [5] and was applied in this study.

$$U(z) = \frac{u^*_{ABL}}{K} \ln\left(\frac{z+z_0}{z}\right) \quad (1)$$

$$k(z) = \alpha \left(I_u(z)U(z)\right)^2 \quad (2)$$

$$\mathcal{E}(z) = \left(\frac{u^{*3}_{ABL}}{\kappa(z+z_0)}\right) \quad (3)$$

$$\omega(z) = \frac{\varepsilon(z)}{C_\mu \mathrm{k(z)}} \tag{4}$$

For ground and building surfaces, standard wall functions developed by Launder & Spalding and sand-grain based roughness modification from Cebeci & Bradshaw's were utilized [19, 20]. The values of roughness parameters, such as sand-grain roughness height, k_s and roughness constant, C_s were computed in accordance to their relation to z_0 which has been obtained through the study of Blocken et al. [21]. The ground sand-grain roughness height, k_s = 0.0006 m was atttained through Eq. (5) where the roughness constant, C_s was set at 0.5. The standard wall functions were also applied for building surface with k_s= 0.

$$k_s = \frac{9.793 z_0}{C_s} \tag{5}$$

Zero static pressure was applied at the symmetry and also the outlet plane. Zero normal gradients and velocity corresponding to zero shear condition was also imposed at the top and side plane.

Solver Settings

In this present research, ANSYS 2020 R1 has been utilized to accomplish the numerical simulations. The 3D steady RANS equation was solved using the SST k-ω turbulence model. This SST k-ω model was chosen for its improved accuracy as compared to the PIV measurements carried out by Karava et al. [13]. The SIMPLE algorithm based on Green Gauss node spatial discretization was used in this study as well. Both convection and viscous terms of the governing equation was also utilized for the second order upwind discretization and pressure interpolation. Convergence was achieved as the scaled residuals recede downward towards 10^{-4}.

Grid Sensitivity Study and Model Validation

Detailed grid sensitivity study was carried out for the reference building model. In order to make sure that the result is grid independent, three different cell counts were used which include 373888 cells (coarse grid), 471660 cells (medium grid), and 913818 cells (fine grid). The simulations were performed utilizing the aforementioned three grids to generate a graph of mean velocity ratio (U/U_{Ref}) of which U refers to 3D streamwise velocity vector, while U_{ref} = 6.97 m/s represents reference wind speed measured at the height of the building (H = 80 mm). Results of these three grids were compared with the PIV experiment results generated by Karava et al. [13] and numerical results obtained by Ramponi and Blocken [5]. Figure 5 demonstrates the PIV measurements by Karava et al. [13] and CFD reference case by Ramponi and Blocken [5] against results obtained from each of the three different cell counts. Grid A, B, and C corresponds to the coarse, medium, and fine grids, respctively. Grid sensitivity study clearly indicates that data generated from the fine mesh (Grid C) simulation best replicates results obtained from wind tunnel experiment by Karava et al. [13] and numerical results by Ramponi and Blocken [5]. Therefore, the fine mesh has been selected for implementation of all successive simulations in this study.

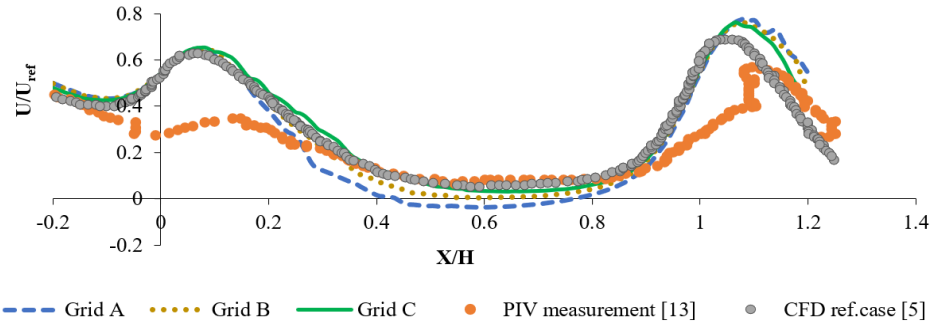

Figure 5. Comparison of the three different cell counts for coarse (Grid A), medium (Grid B) & fine (Grid C) with result of PIV measurement by Karava et al. [13] and numerical results by Ramponi and Blocken [5]

Furthermore, compariosn is made between results obtained from the reference case against that of the findings by Ramponi and Blocken [5] for the purpose of validating the correctness of the simulation results. As shown in Figure 6, the validation was performed by using the contours by Ramponi and Blocken [5]. Through this model validation, it shows that the contour obtained from the simulation in this study looks similar to that obtained by Ramponi and Blocken [5]. Additionally, the wind tunnel experimental works as well as the CFD simulations carried out by Tominaga et al. [8] were also applied to further validate the gable roof model. This gable roof model was develeoped with neither windows nor roof openings for purpose of validation. Streamlines and pressure coeffiecient around the simulated models were then matched against the numerical results by Tominaga et al. [8].

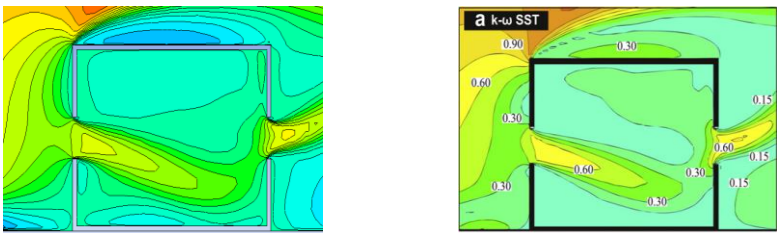

(a) (b)

Figure 6. Validation based on velocity contour: (a) simulation result and (b) result by Ramponi and Blocken [5]

Figures 7 and 8 compare both streamlines as well as distribution of pressure coefficient (Cp) between the simulation result and result by Tominaga et al. [8]. Result demonstrates a substantial recirculation region at the back of the building and a slight recirculation region located at the bottom edge of the building's windward side. Some positive pressure has been detected at the frontal region of the simulation model due to the obstruction caused by the building. Negative peaks at the frontal edge of the model were observed to be present in both cases as well. Further observation of Figure 7 also found a wake at the back of the simulation model which is greater in comparison to the result by Tominaga et al. [8]. This is due to the fact that the simulation model was based on the SST $k-\omega$ turbulence model whereas the result by Tominaga et al. [8] was simulated based on the RNG $k-\varepsilon$ model. These two RANS models perform differently in turbulence prediction. While accuracy of the predictions can be substantially improved by systematic optimization of the closure coefficients in the RANS models [22], this work is not within the scope for this research. Therefore, this simulation model has been modified accordingly for subsequent simulations.

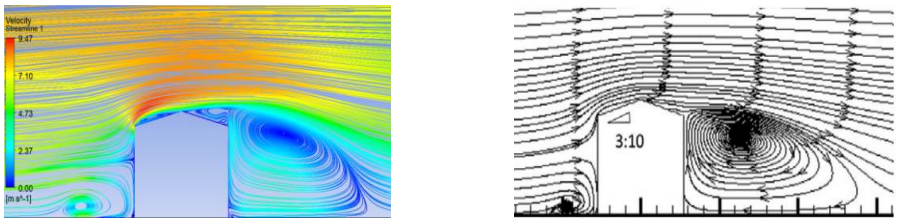

(a) (b)

Figure 7. Validation based on the streamlines (a) simulation result of 15º roof pitch and (b) result by Tominaga et al. for roof pitch of 16.6º [8]

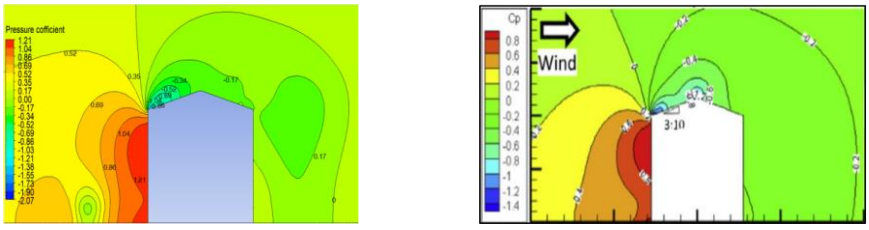

(a) (b)

Figure 8. Validation based on the pressure coefficient (Cp) contour (a) simulation result of 15º roof pitch and (b) result by Tominaga et al. [8]

RESULTS AND DISCUSSION

Streamlines

Table 2 tabulates the normalized velocity streamlines for different roof pitches & obstacle heights of 40, 50, 60 & 70 mm. Findings by Tominaga et al. [8] demonstrates that an increase in roof pitch contributes to greater recirculation regions at the leeward side of the building and causes the central region of the recirculation eddy at the back of the building to move upwards and away from the building. However, the presence of internal obstacle and openings such as window and roof would interrupt the recirculation flow behind the model. Analysis of the results indicate an evident alteration of the flow field amid roof pitch of 15° and 25°. Reverse flow was not detected at the back of the building for roof pitch of 15°, but develops and grows bigger at roof pitches of 25°, 35° & 45°. The corresponding critical roof pitch from this study is therefore consistent with the critical roof pitch of 18° whereby noticeable change of flow starts to occur around the gable roof building [23]. Flow velocity was observed to be increasing with the increase in roof pitch. This velocity distribution would also be affected if an internal obstacle is encountered upon entering the building. Within the building, the airflow entering from the window opening would be immediately deflected downward due to the opening location and formation of the recirculation zone in front of the building. Whenever this airflow approaches the obstacle in its path, a recirculation of flow has been observed in front of the obstacle due to the wind block. In addition, flow entering the building would also be deflected slightly upward due to the upstream upward flow at the roof opening, which is consistent with the

findings from Karava et al. [13]. Furthermore, it has been noticed that airflow at the windward opening would change its direction due to the gradual increase in obstacle height.

Spatial Distribution of Pressure Coefficient

Table 3 shows the spatial distribution of pressure coefficient around a building having different gable roof pitches as well as different obstacle heights namely that of 40, 50, 60 & 70 mm. Observations show that the windward wall of the building has a greater positive peak value of pressure coefficient as roof pitch increases due to more blockage caused by the steeper roof. Meanwhile, negative peak value is noticed at the windward edge and the ridge region of the 15° gable roof as a result of flow separation. This negative peak value would however diminish and shift towards the roof ridge with increasing roof pitch due to enhanced impinging effect. On the contrary, the negative value near the leeward region of the roof becomes larger with increasing roof pitch inclination, which in turn develops a larger wake formation region. The enlarging negative pressure coefficient is a consequence of flow separation at the roof ridge. Furthermore, an increase in obstacle height would trap more air, hence increasing the internal pressure of the building. Nevertheless, this internal pressure would decrease as roof pitch increases thereby proving the theory that induced pressure difference has significant interrelation with wind speed across the building, obeying the Bernoulli principle.

Table 2. Normalized velocity (U/U_{ref}) streamlines of various roof pitch and obsctacle height

Cases	Legend	15°	25°	35°	45°
Obstacle height 40 mm	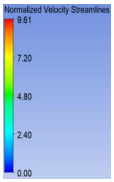	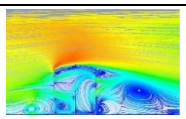	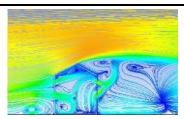	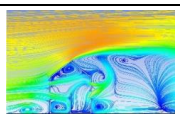	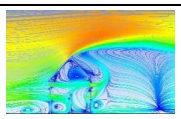
Obstacle height 50 mm		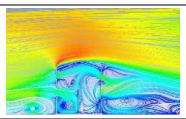	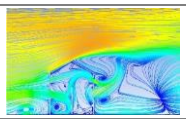	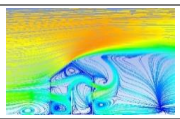	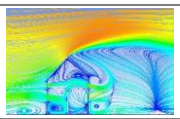
Obstacle height 60 mm		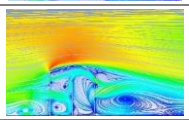	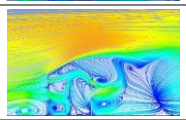	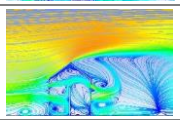	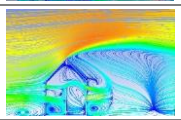
Obstacle height 70 mm		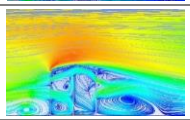	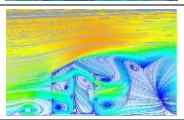	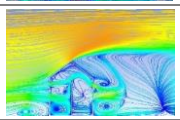	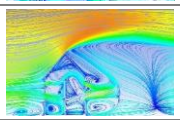

Table 3. Spatial distribution of pressure coefficient for various roof pitch and obstacle height

Cases	Legend	15°	25°	35°	45°
Obstacle height 40 mm	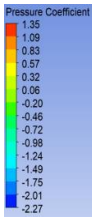	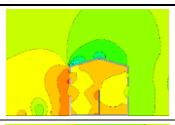			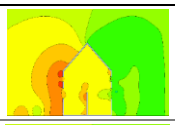
Obstacle height 50 mm		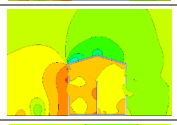			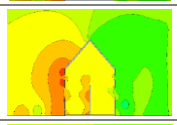
Obstacle height 60 mm		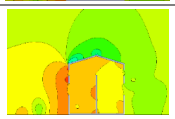	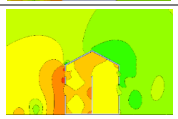	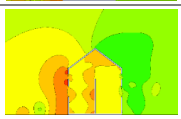	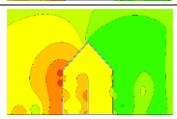
Obstacle height 70 mm		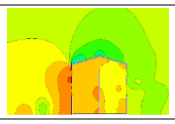			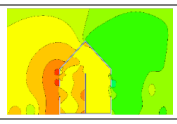

Mean Velocity Profile

Figure 9 illustrates both inlet as well as outlet profiles with regards to the dimensionless streamwise mean velocity, U/U_{ref} at the roof opening (RO) and window opening (WO) regions of the building. Result demostrates a velocity increase at both roof and window openings as roof pitch increases. Wind speed increases as it enters and exits the building due to presence of the pressure differential between the interior and exterior regions. Notable difference can be observed in Figure 9 (a), between roof pitch of 25º & 45º for the case of 40 mm obstacle height. However, a constant velocity increase has also been noticed between roof pitch of 15°, 25°, 35° & 45° in Figure 9 (c), (e), and (g), at the windward window

openings of the gable roof having 50, 60 & 70 mm obstacle heights respectively. Observation also shows the U/U_{ref} profile at the windward roof opening constantly changes for all the obstacle cases when upon increase of roof pitch as shown in Figure 9 (a), (c), (e), and (g). Additionally, a constant increase in velocity of the window outlet is observed at 50, 60 & 70 mm obstacle heights with the steepness of roof pitch as illustrated in Figure 9 (d), (f), and (h), contrasting to the abrupt decrease observed at 45° roof pitch with 40 mm obstacle height as illustrated in Figure 9 (b). Also as indicated in Figure 9 (b), (d), (f), and (h), a constant increase of the velocity is observed at the roof outlet of all obstacle cases with the increment in roof pitch, whereby a prominent velocity increase is particularly noticeable at both 40 mm and 50 mm obstacle heights and 45° roof pitch as shown in Figure 9 (b) and (d). In short, velocity profile of the roof outlet gradually changes with increase in obstacle height. Simulations results hereby demonstrate a strong reliance of U/U_{ref} on the roof pitch and obstacle height.

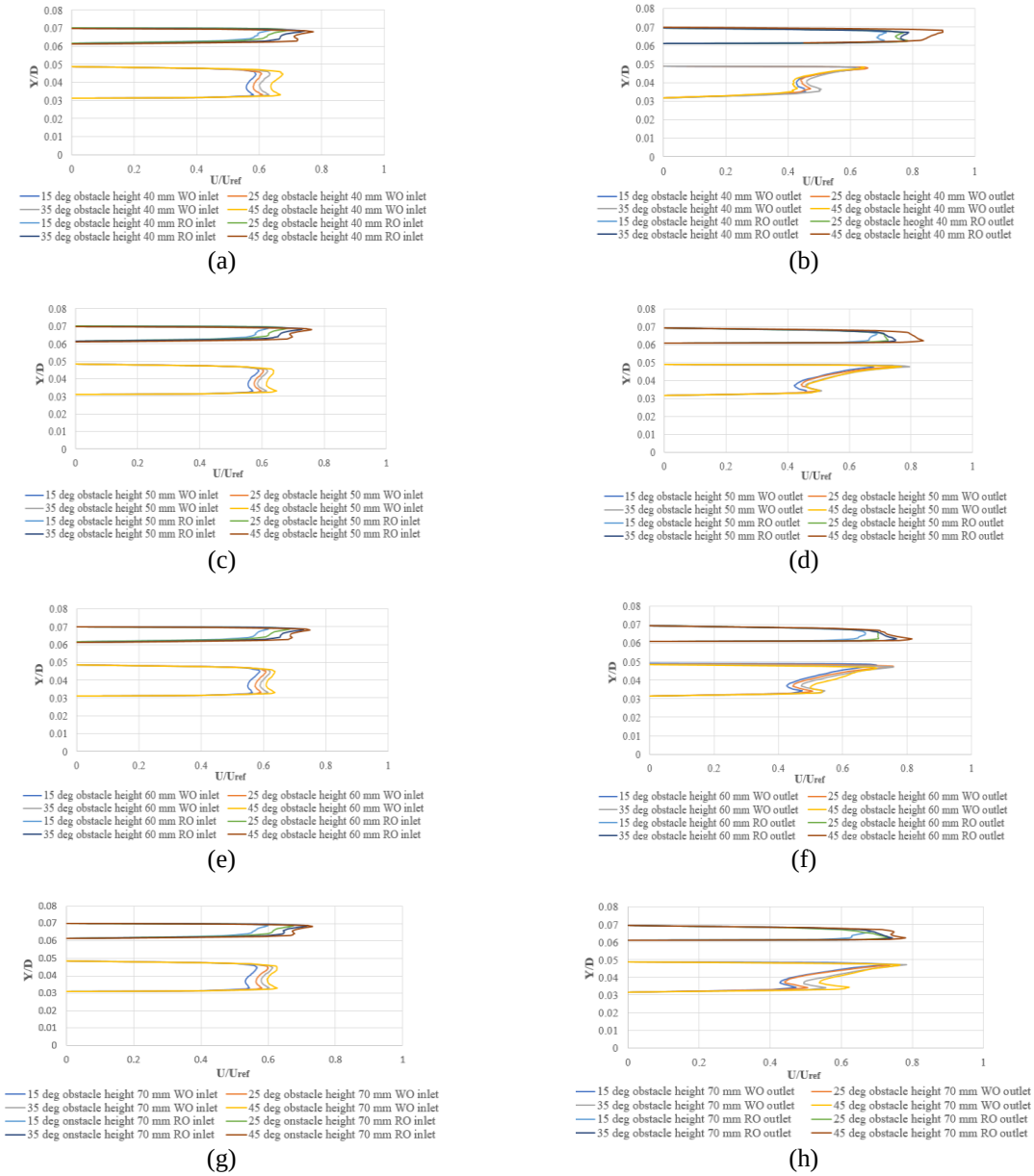

Figure 9. Velocity profile of roof opening (RO) and window opening (WO) with different internal obstacle height of: (a) 40 mm, (c) 50 mm, (e) 60 mm, (g) 70 mm at the windward openings and (b) 40 mm, (d) 50 mm, (f) 60 mm, and (h) 70 mm at the leeward openings

Ventilation Rate

A simple relationship can be deployed to calculate the building ventilation rate. The ventilation rate of such isolated low rise naturally ventilated building can be calculated as follows [24]:

$$C_p = \frac{p - p_r}{\frac{1}{2}\rho V_{ref}^2} \tag{6}$$

$$CQ = C_d V_{ref} \sqrt{\Delta C_p} \quad (7)$$

$$C_a = \frac{CQ}{(1+CQ)} \quad (8)$$

$$Q = C_a V_{ref} A_e \quad (9)$$

Equation (6) can be applied to calculate the pressure coefficient, C_P, of which P represents the pressure at designated opening, P_r represents the reference free stream static pressure, $\rho = 1.225$ kg/m^3 represents the air density, and $V_{ref} = 6.97$ m/s. This pressure coefficient calculated at both windward and leeward openings were used into Eq. (7) to compute the estimated flow coefficient CQ, of which $C_d = 0.62$ represents the discharge coefficient for a sharp opening while Δ_{CP} represents the pressure coefficient differential of the inlet and outlet openings. Subsequently, Eq. (9) which is originated from the Bernoulli's principle can be used to compute the ventilation rate by multiplying the actual flow coefficient C_a, with V_{ref}, and effective area of opening A_e. The effective area (A_e) was calculated to be 1.242×10^{-3} m^2 in this study.

Figure 10 shows the ventilation rate amongst the four different roof pitch with various obstacle heights. Result demonstrates that ventilation rate increases as the roof pitch becomes higher. At 40 mm obstacle height, a higher ventilation rate differential of 1.47% is observed when roof pitch increased from 15º to 25º. For the same obstacle height, this differential increased by only 0.84% as roof pitch increases to 35º, and 1.34% as the roof pitch further increases to 45°. All other obstacle height cases adopt a similar pattern whereby ventilation rate differential is highest between the 15° and 25° roof pitch angle, and lowest between the 25° and 35° roof pitch angle. At 50 mm, 60 mm & 70 mm obstacle heights, the ventilation rate differentials between 15° and 25°, 25° and 35°, as well as 35° to 45° are measured to be 1.22%, 0.99%, 1.08%; 1.51%, 0.78%, 0.94%; and 1.87%, 0.48%, 0.85%, respectively. This is due to the difference in pressure between the inside and outside of the building. This indoor-outdoor pressure difference induces wind flow into the building at an escalating velocity via the openings. The greater the wind speed flowing into a building at increasing roof pitch in turn generate increased ventilation rate. Additionally, internal obstacle height has also been observed to have a significant impact on ventilation rate. The ventilation rate gradually decreases with the increase in obstacle height because a higher obstacle height contributes to more blockage of airflow. Result shown in Figure 10 is in good agreement with previous literature, veryfying the finding of which ventilation rate is inversely proportionate to obstacle height [25]. While ventilation rate is highest at 40 mm obstacle height, it became the lowest when the obstacle height is increased by 75%.

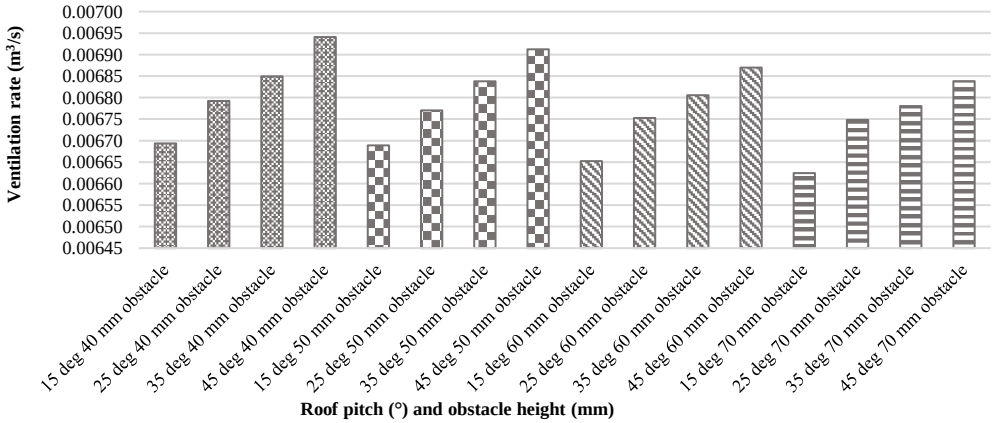

Figure 10. Ventilation rate (m^3/s) of gable roof with various roof pitch and obstacle height

CONCLUSION

In this current study, airflow characteristics around and within an isolated building with gable roof of different roof pitch (15º, 25º, 35º, & 45°) and varying internal obstacle heights (40, 50, 60, & 70 mm) were investigated and analysed using 3D steady-state RANS equation with SST $k - \omega$ turbulence model. The validation of the model has been accomplished and verified to be consistent with the findings of previous studies. Numerical result shows that the velocity streamlines, pressure coefficient, mean velocity ratio, and ventilation rate have high significant dependence on the roof pitch as well as internal obstacle height. The recirculation region behind the building has a tendency of moving upward and increase in size as the roof pitch increases. The air flow inside the building would also gradually change its direction with an increase in obstacle height. On the contrary, negative peaks are observed at the windward edge due to flow separation. Pressure inside the building also increases at greater obstacle height due to increased wind blocking effect. Contrastingly, the same pressure decreases with increment in roof pitch due to increased flow velocity. In addition, the velocity profile of all obstacle cases at the windward as well as leeward openings tends to increase along with the steepness of roof pitch due to exterior and interior pressure difference. Ventilation rate, on the other hand, increases with an increase in roof pitch, but decreases gradually with an increase in obstable height. With reference to all the findings above, it can be summarized that the gable roof with steeper roof pitch and lower obstacle height is recommended to achieve improved natural ventilation for a building. However, this research is specific to solely a single wind speed and a fixed obstacle

position of that located only at the centreline of the building. As ventilation rate would also be influenced by having different wind speed values and obstacle positions, such factors can be further investigated in future study.

REFERENCES

[1] Department of Malaysian Standard, "MS 1525:2014 Energy Efficiency and Use of Renewable Energy for Non Residential Buildings Code of Practice," *Stand. Malaysia 2014*, pp. 1–74, 2014.

[2] C. H. Lim, Omidreza Saadatian, K. Sopian, M. Yusof Sulaiman, S. Mat, E. Salleh, and K.C. Ng, "Design configurations analysis of wind-induced natural ventilation tower in hot humid climate using computational fluid dynamics," *Int. J. Low-Carbon Technol.*, vol. 10, no. 4, pp. 332–346, 2015, doi: 10.1093/ijlct/ctt039.

[3] M. N. Khan and I. Janajreh, "Transevaporative cooling performance of a three-sided wind catcher," *Jordan J. Mech. Ind. Eng.*, vol. 11, no. 4, pp. 225–233, 2017.

[4] L. K. Moey, M. F. Kong, V. C. Tai, T. F. Go, and N. M. Adam, "Effects of roof configuration on natural ventilation for an isolated building," *J. Mech. Eng. Sci.*, vol. 15, no. 3, pp. 8379–8389, 2021, doi: 10.15282/jmes.15.3.2021.15.0659.

[5] R. Ramponi and B. Blocken, "CFD simulation of cross-ventilation for a generic isolated building: Impact of computational parameters," *Build. Environ.*, vol. 53, pp. 34–48, 2012, doi: 10.1016/j.buildenv.2012.01.004.

[6] J. Kindangen, G. Krauss, and P. Depecker, "Effects of roof shapes on wind-induced air motion inside buildings," *Build. Environ.*, vol. 32, no. 1, pp. 1–11, 1997, doi: 10.1016/S0360-1323(96)00021-2.

[7] L. K. Moey, N. M. Adam, and K. A. Ahmad, "Effect of venturi-shaped roof angle on air change rate of a stairwell in tropical climate," *J. Mech. Eng.*, vol. SI 4, no. 4, pp. 135–150, 2017.

[8] Y. Tominaga, S. ichi Akabayashi, T. Kitahara, and Y. Arinami, "Air flow around isolated gable-roof buildings with different roof pitches: Wind tunnel experiments and CFD simulations," *Build. Environ.*, vol. 84, pp. 204–213, 2015, doi: 10.1016/j.buildenv.2014.11.012.

[9] X. Zhou, Y. Zhang, L. Kang, and M. Gu, "CFD simulation of snow redistribution on gable roofs: Impact of roof slope," *J. Wind Eng. Ind. Aerodyn.*, vol. 185, pp. 16–32, 2019, doi: 10.1016/j.jweia.2018.12.008.

[10] M. G. Badas, S. Ferrari, M. Garau, and G. Querzoli, "On the effect of gable roof on natural ventilation in two-dimensional urban canyons," *J. Wind Eng. Ind. Aerodyn.*, vol. 162, pp. 24–34, 2017, doi: 10.1016/j.jweia.2017.01.006.

[11] L. K. Moey, M. F. Kong, V. C. Tai, T. F. Go, and N. M. Adam, "Effect of gable roof angle on natural ventilation for an isolated building," *Jordan J. Mech. Ind. Eng.*, vol. 15, no. 3, pp. 291–300, 2021.

[12] C. R. Chu and B. F. Chiang, "Wind-driven cross ventilation with internal obstacles," *Energy Build.*, vol. 67, pp. 201–209, 2013, doi: 10.1016/j.enbuild.2013.07.086.

[13] P. Karava, T. Stathopoulos, and A. K. Athienitis, "Airflow assessment in cross-ventilated buildings with operable façade elements," *Build. Environ.*, vol. 46, no. 1, pp. 266–279, 2011, doi: 10.1016/j.buildenv.2010.07.022.

[14] J. Franke, A. Hellsten, H. Schlünzen, and B. Carissimo, "Best practice guideline for the CFD simulation of flows in the urban environment," *COST action*, vol. 44, no. May, pp. 1–52, 2007.

[15] Y. Tominaga, A. Mochida, R. Yoshie, H. Kataoka, T. Nozu, M. Yoshikawa, and T. Shirasawa, "AIJ guidelines for practical applications of CFD to pedestrian wind environment around buildings," *J. Wind Eng. Ind. Aerodyn.*, vol. 96, no. 10–11, pp. 1749–1761, 2008, doi: 10.1016/j.jweia.2008.02.058.

[16] Z. Krishna, P. Gandhar, Balasubramanyam, A. Varghese, ANSYS Inc, K. Zore, B. Sasanapuri, G. Parkhi, and A. Varghese, "Ansys mosaic poly-hexcore mesh for high-lift aircraft configuration," *21 st Annu. CFD Symp.*, no. September, pp. 1–11, 2019.

[17] Panagiota Karava, "Airflow prediction in buildings for natural ventilation design: Wind tunnel measurements and simulation," *Concordia Univ.*, no. May, 2008.

[18] R. Ramponi and B. Blocken, "CFD simulation of cross-ventilation flow for different isolated building configurations: Validation with wind tunnel measurements and analysis of physical and numerical diffusion effects," *J. Wind Eng. Ind. Aerodyn.*, vol. 104–106, pp. 408–418, 2012, doi: 10.1016/j.jweia.2012.02.005.

[19] B. E. Launder and D. B. Spalding, "The numerical computation of turbulent flows," *Comput. Methods Appl. Mech. Eng.*, vol. 3, no. 2, pp. 269–289, 1974, doi: 10.1016/0045-7825(74)90029-2.

[20] T. Cebeci and P. Bradshaw, "Momentum transfer in boundary layers," *New York Hemisph. Publ. Corp.*, pp. 377–386, 1977.

[21] B. Blocken, T. Stathopoulos, and J. Carmeliet, "CFD simulation of the atmospheric boundary layer: wall function problems," *Atmos. Environ.*, vol. 41, no. 2, pp. 238–252, 2007, doi: 10.1016/j.atmosenv.2006.08.019.

[22] M. Shirzadi, P. A. Mirzaei, and M. Naghashzadegan, "Improvement of k-epsilon turbulence model for CFD simulation of atmospheric boundary layer around a high-rise building using stochastic optimization and Monte Carlo Sampling technique," *J. Wind Eng. Ind. Aerodyn.*, vol. 171, pp. 366–379, 2017, doi: 10.1016/j.jweia.2017.10.005.

[23] Y. Takano and P. Moonen, "On the influence of roof shape on flow and dispersion in an urban street canyon," *J. Wind Eng. Ind. Aerodyn.*, vol. 123, pp. 107–120, 2013, doi: 10.1016/j.jweia.2013.10.006.

[24] M. Swami and S. Chandra, "Procedures for calculating natural ventilation airflow rates in buildings," *ASHRAE Final Rep. FSEC-CR-163-86*, p. 130, 1987.

[25] S. Hawendi and S. Gao, "Impact of an external boundary wall on indoor flow field and natural cross-ventilation in an isolated family house using numerical simulations," *J. Build. Eng.*, vol. 10, pp. 109–123, 2017, doi: 10.1016/j.jobe.2017.03.002.